INTERNATIONAL JOURNAL FOR NUMERICAL METHODS IN ENGINEERING
*Int. J. Numer. Meth. Engng* 2002; **55**:1373–1390 (DOI: 10.1002/nme.531)

# The maximum principle violations of the mixed-hybrid finite-element method applied to diffusion equations

H. Hoteit[1,2], R. Mosé[3,*,†], B. Philippe[2], Ph. Ackerer[1] and J. Erhel[2]

[1]*Institut de Mécanique des Fluides, Univ. Louis Pasteur de Strasbourg, CNRS/UMR 7507, 2 rue Boussingault, F-67000 Strasbourg, France*
[2]*IRISA-INRIA,Campus de Beaulieu, 35042 Rennes Cedex, France*
[3]*Ecole Nationale du Génie de l'Eau et de l'Environnement, 1 Quai Koch, 67070 Strasbourg, France*

SUMMARY

The abundant literature of finite-element methods applied to linear parabolic problems, generally, produces numerical procedures with satisfactory properties. However, some initial–boundary value problems may cause large gradients at some points and consequently jumps in the solution that usually needs a certain period of time to become more and more smooth. This intuitive fact of the diffusion process necessitates, when applying numerical methods, varying the mesh size (in time and space) according to the smoothness of the solution. In this work, the numerical behaviour of the time-dependent solutions for such problems during small time duration obtained by using a non-conforming mixed-hybrid finite-element method (MHFEM) is investigated. Numerical comparisons with the standard Galerkin finite element (FE) as well as the finite-difference (FD) methods are checked. Owing to the fact that the mixed methods violate the discrete maximum principle, some numerical experiments showed that the MHFEM leads sometimes to non-physical peaks in the solution. A diffusivity criterion relating the mesh steps for an artificial initial–boundary value problem will be presented. One of the propositions given to avoid any non-physical oscillations is to use the mass-lumping techniques. Copyright © 2002 John Wiley & Sons, Ltd.

KEY WORDS: parabolic problem; mixed-hybrid finite-element method; discrete maximum principle; refinement; mass lumping

## 1. INTRODUCTION

Many environmental problems, in particular the transport of pollutants by underground water, have pressed upon the attention to develop new methods for more precise representative simulations. Subsequently, numerical modelling has played an increasing role to solve such physical processes. Despite the fact that the mathematical models delineating the transport problems are described by coupled systems of non-linear partial differential equations, in

*Correspondence to: R. Mosé, Ecole Nationale du Génie de l'Eau et de l'Environnement, 1 Quai Koch, 67070 Strasbourg, France
†E-mail: rmose@engees.u-strasbg.fr

*Received 15 May 2001*
*Revised 3 December 2001*
*Accepted 9 January 2002*

Copyright © 2002 John Wiley & Sons, Ltd.

this paper we are restricted to the linear diffusion equation since the focus is to give a numerical study of the approximated solution attained by the MHFE method. Nevertheless, this work is of importance even for the non-linear advection–diffusion problems since one of the approaches to solve such problems is by using the time-splitting operator technique, i.e. advection and dispersion operators are treated separately. Generally, the MHFEM is voted to solve the diffusion part [1].

For the unknown pressure scalar function $p=p(x,t)$ and velocity vector function $u=u(x,t)$, we consider the mass conservation equation and Darcy's law which are given as follows:

$$s\frac{\partial p}{\partial t}+\nabla u=f \qquad \text{in } \Omega\times(0,T] \tag{1}$$

$$p(x,0)=p^0(x) \quad \text{in } \Omega \tag{2}$$

$$p=p^{\mathrm{D}} \qquad \text{on } \Gamma^{\mathrm{D}}\times(0,T] \tag{3}$$

$$u\cdot=q^{\mathrm{N}} \qquad \text{on } \Gamma^{\mathrm{N}}\times(0,T] \tag{4}$$

the so-called Darcy velocity $u$ is given via

$$u=-\mathscr{K}\nabla p \quad \text{in } \Omega\times(0,T] \tag{5}$$

where $\Omega$ is a bounded domain in $R^d$ $(d=1,\ldots,3)$ with boundary $\partial\Omega=\Gamma^{\mathrm{D}}\cup\Gamma^{\mathrm{N}}$; $\mathscr{K}=\mathscr{K}(x)$ is the conductivity, it is assumed to be a diagonal tensor with components in $L^\infty(\Omega)$; $v$ indicates the outward unit normal vector along $\partial\Omega$; $f=f(x,t)\in L^2(\Omega)$ represents the sources; $s=s(x)$ is the storage coefficient; $p^{\mathrm{D}}(x,t)$ and $q^{\mathrm{N}}(x,t)$ are, respectively, the Dirichlet and Neumann boundary conditions.

It should be noted that the above parabolic, initial–boundary value problem can also model many other physical phenomena like heat transfer, chemical transport and electromagnetic current [2]. For the reason of similarity, the fluid flow equation in porous media is chosen to be studied.

The finite-element methods have been the preferred tools over the finite-difference methods due to their simple physical interpretation and their flexibility dealing with irregular geometrical domains. In modelling flow in porous media, it is essential to utilize a discretization method which satisfies the physics of the problem, i.e. conserves mass locally and preserves continuity of fluxes. The Raviart–Thomas mixed finite-element method of lowest order satisfies these properties. Moreover, both the pressure and the velocity are approximated with the same order of convergence (see, e.g., References [3–5]). One of the inconvenient properties of this method is that it leads to an indefinite linear system, so its resolution cannot be achieved by simple robust algorithms like Choleski or conjugate gradient methods. Furthermore, the number of unknowns is relatively quite large since both the pressure on each element and the flux through each edge have to be calculated simultaneously [6]. The mixed-hybrid formulation was introduced as a method for solving the mixed finite-element linear system [7]. Moreover, this technique provides more information about the pressure since the degrees of freedom of the pressure on the edges are computed as well.

Numerous works showed the accuracy and the efficiency of this method applied to the stationary diffusion problem [8–10]. However, numerical comparisons presented in many papers like [11, 12], which showed the upper hand of the MHFEM applied to the parabolic problem with regard to other classical methods, took an implicit supposition of at least one

Copyright © 2002 John Wiley & Sons, Ltd. 

of these two cases: (i) smooth initial and boundary values, (ii) sufficient long interval of simulation time $(0, T]$. Discordantly, in this work we show that the MHFEM applied to some particular initial-boundary value diffusion problems leads to relatively erroneous results compared with solutions obtained by the classical FE or FD methods. It is proved that under assumptions of smoothness of initial and boundary conditions, optimal convergence for the pressure and the velocity is obtained (see, e.g., References [3, 4, 13, 14]). In our study here, we show, by numerical experiments, that if the assumption of smoothness is omitted an oscillatory solution is obtained at some points of large gradient.

The fact that the mixed methods do not obey the discrete maximum principle is well known [4]. In the work presented in Reference [15], it is found that the MHFEM applied to semiconductor device equations violates the discrete maximum principle. This problem is time-independent convection–diffusion problem. However, in this work we study the MHFEM applied to an groundwater flow problem which is a time-dependent purely diffusive problem.

An outline of the paper is as follows. In Section 2, the formulation of the MHFEM corresponding to the Raviart–Thomas space of lowest order is reviewed. Numerical analyses of the solution of an artificial well-posed initial–boundary value problem are discussed in Section 3 where we compare the approximated solutions with the exact one. In Section 4 we show that, unlike the FD method, the MHFEM conditionally satisfies the discrete maximum principle. Before ending with a conclusion, we give in Section 5 some alternative propositions to prevent the non-physical oscillations in the solutions attained by the MHFE method.

## 2. THE HYBRIDIZED MIXED FINITE-ELEMENT METHOD

We restrict our discussion to the two-dimensional case: the three-dimensional case follows in a similar manner. The polygonal domain $\Omega$ is discretized into a mesh $\mathcal{Q}_h$ consisting of parallelograms or triangles where $h$ denotes the mesh parameter. In practice, quadrangles are restricted to be parallelograms since these can be generated from the reference element by affine transformations. Throughout this paper, we denote by $\mathcal{E}_h$ the set of edges of the grid not belonging to $\Gamma^{\mathrm{N}}$, $N_{\mathcal{E}}$ is the cardinal of $\mathcal{E}_h$ and $N_{\mathcal{Q}}$ is the number of discretized elements.

In the mixed finite-element method, Darcy's law and the mass conservation equation are approximated individually subsequently; we get additionally the Darcy velocity $u$ as an unknown function. In the following, we present the approximation spaces of our unknowns, the discretization of Darcy's law and that of the mass conservation equation as well as the derived algebraic system to solve.

### *2.1. Approximation spaces*

The essential idea of the MFE methods is to approximate simultaneously the pressure and its gradient. The simplest case of approximation, which is by means of the space of Raviart–Thomas of the lowest order $\mathrm{RT}_0$, will be presented in brief. For more details see References [3, 4, 13, 16].

The finite approximation spaces of the pressure $p_h$ and the velocity $u_h$ are the two finite-dimensional spaces $\mathcal{M}(\mathcal{Q}_h)$ and $\mathcal{V}(\mathcal{Q}_h)$, respectively.

Copyright © 2002 John Wiley & Sons, Ltd. 

$\mathscr{M}(\mathscr{Q}_h)$ is the space of piecewise constant function on each element of $\mathscr{Q}_h$, it is given by

$$\mathscr{M}(\mathscr{Q}_h)=\{\varphi\in L^2(\Omega)\,|\,\varphi/_K\in\mathscr{P}_0(K),K\in\mathscr{Q}_h\}$$

where $\mathscr{P}_d(K)$ is the space of polynomials of total degree $d$ defined on $K$.

$\mathscr{V}(\mathscr{Q}_h)$ is given by the Raviart–Thomas space $\mathrm{RT}_0(\mathscr{Q}_h)$:

$$\mathscr{V}(\mathscr{Q}_h)=\mathrm{RT}_0(\mathscr{Q}_h)=\{\chi\in L^2(\Omega)\,|\,\chi/_K\in\mathrm{RT}_0(K),K\in\mathscr{Q}_h\}$$

where $\mathrm{RT}_0(K)$ stands for the lowest Raviart–Thomas element,

$$\mathrm{RT}_0(K)=\begin{cases}\{\phi\in(\mathscr{P}_1(K))^2\,|\,\phi=(a+bx_1,c+bx_2),\ a,b,c\in\mathbb{R}\} & \text{if } K \text{ is triangle}\\ \{\phi\in(\mathscr{P}_1(K))^2\,|\,\phi=(a+bx_1,c+dx_2),\ a,b,c,d\in\mathbb{R}\} & \text{if } K \text{ is parallelogram}\end{cases}$$

The hybridization technique tends to enforce the continuity of the normal component of $u_h$ across the interelement boundaries by using the Lagrange multiplier spaces

$$\mathscr{N}(\mathscr{E}_h)=\{\lambda\in L^2(\mathscr{E}_h)\,|\,\lambda/_E\in\mathscr{P}_0(E)\ \forall E\in\mathscr{E}_h\}$$

$$\mathscr{N}_{g,D}(\mathscr{E}_h)=\{\lambda\in\mathscr{N}(\mathscr{E}_h)\,|\,\lambda=g\ \text{ on }\ \Gamma^{\mathrm{D}}\}$$

Now we introduce $tp_h$ a new degree of freedom approximating the traces of the pressure on the edges of the mesh. Thus the MHFE formulation reads as: Find $(u_h, p_h, tp_h)\in\mathscr{V}(\mathscr{Q}_h)\times\mathscr{M}(\mathscr{Q}_h)\times\mathscr{N}_{p^{\mathrm{D}},D}(\mathscr{E}_h)$ such that

$$\begin{aligned}
&\int_\Omega(\mathscr{K}^{-1}u_h)\cdot\chi_h\,\mathrm{d}x+\sum_{K\in\mathscr{Q}_h}\int_{\partial K}tp_h v_K\cdot\chi_h\,\mathrm{d}\ell=\sum_{K\in\mathscr{Q}_h}\int_K p_h\nabla\cdot\chi_h\,\mathrm{d}x && \forall\chi_h\in\mathscr{V}(\mathscr{Q}_h)\\
&\int_\Omega s\,\frac{\partial p_h}{\partial t}\,\varphi_h\,\mathrm{d}x+\int_\Omega\nabla\cdot u_h\varphi_h\,\mathrm{d}x=\int_\Omega f\varphi_h\,\mathrm{d}x && \forall\varphi_h\in\mathscr{M}(\mathscr{Q}_h) \qquad (6)\\
&\sum_{K\in\mathscr{Q}_h}\int_{\partial K}u_h\cdot v_K\lambda_h\,\mathrm{d}\ell=\int_{\partial\Omega}q^{\mathrm{N}}\lambda_h\,\mathrm{d}\ell && \forall\lambda_h\in\mathscr{N}_{0,D}(\mathscr{E}_h)
\end{aligned}$$

### 2.2. *Local basis functions*

As a matter of fact, any irregular element $K$ can be mapped from a reference element $\hat{K}$ (as shown in Figure 1) by using an affine transformation (see, e.g., References [13, 16, 17]). This mapping is defined as

$$\begin{aligned}\hat{K} &\mapsto K\\ \hat{x} &\mapsto x=T_K\hat{x}+b_K\end{aligned}$$

Subsequently, $\mathscr{V}(K)=RT_0(K)$ could be written as

$$\mathscr{V}(K)=\frac{1}{J_K}\,T_K\mathscr{V}(\hat{K})$$

where $T_K$ is the transformation matrix, $J_K=\det(T_K)$ is the Jacobian and $b_K$ is a point in $K$. The Raviart–Thomas basis functions of $\mathscr{V}(\hat{K})$, defined on the reference element, are defined as follows:

Copyright © 2002 John Wiley & Sons, Ltd. 

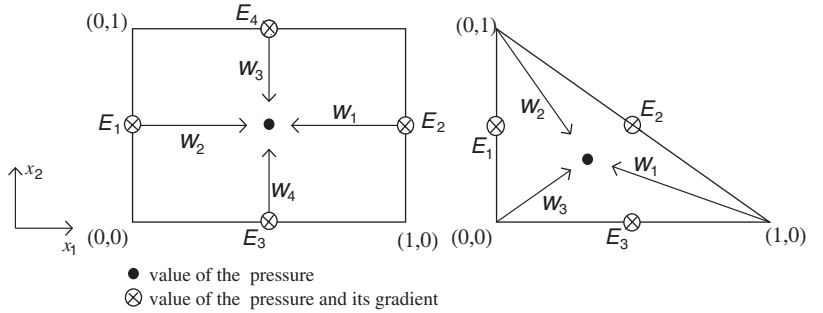


Figure 1. The approximated unknowns and the basis functions on the reference elements.

If $K$ is a triangle (as depicted in Figure 1), a choice for a basis of the three-dimensional space $\mathscr{V}(\hat{K})$ is

$$\hat{w}_{\hat{K},E_1} = \begin{bmatrix} \hat{x}_1 - 1 \\ \hat{x}_2 \end{bmatrix}, \quad \hat{w}_{\hat{K},E_2} = \begin{bmatrix} \hat{x}_1 \\ \hat{x}_2 - 1 \end{bmatrix}, \quad \hat{w}_{\hat{K},E_3} = \begin{bmatrix} \hat{x}_1 \\ \hat{x}_2 \end{bmatrix} \tag{7}$$

On the other hand, if $K$ is a rectangle (see Figure 1), $\mathscr{V}(\hat{K})$ becomes a four-dimensional space with the basis functions

$$\hat{w}_{\hat{K},E_1} = \begin{bmatrix} \hat{x}_1 - 1 \\ 0 \end{bmatrix}, \quad \hat{w}_{\hat{K},E_2} = \begin{bmatrix} \hat{x}_1 \\ 0 \end{bmatrix}$$

$$\hat{w}_{\hat{K},E_3} = \begin{bmatrix} 0 \\ \hat{x}_2 - 1 \end{bmatrix}, \quad \hat{w}_{\hat{K},E_4} = \begin{bmatrix} 0 \\ \hat{x}_2 \end{bmatrix} \tag{8}$$

One can easily verify that for every $\chi_K = \sum_{E \subset \partial K} q_{K,E} w_{K,E} \in \mathscr{V}(K)$ and $K \in \mathscr{Q}_h$, the following properties are satisfied:

(1) $\nabla \cdot \chi_K$ is constant over $K$.
(2) $v_{K,E} \cdot \chi_K = q_{K,E}$ is constant on each $E \subset \partial K$.

Hence $u_K$ is uniquely determined by the normal fluxes $q_{K,E} = u_K \cdot v_{K,E}$ on the edges of $K$, where $v_{K,E}$ denotes the outer normal vector on $E$ with respect to $K$.

### 2.3. Approximation equations

The finite-dimensional space $\mathscr{V}(\mathscr{Q}_h)$ is spanned by linearly independent vectorial basis functions $w_{K,E}$, $E \subset \partial K$, $K \in \mathscr{Q}_h$, such that $w_{K,E}$ has its support in $K$ ($\mathrm{supp}(w_{K,E}) \subseteq K$) and

$$\int_{E'} w_{K,E} \cdot v_K \, \mathrm{d}\ell = \delta_{EE'}, \quad E, E' \subset \partial K$$

These functions can be chosen the local bases functions given in Equation (7) or (8). Thus, a function $u_h \in \mathscr{V}(\mathscr{Q}_h)$ has three degrees of freedom per element which are the fluxes across

Copyright © 2002 John Wiley & Sons, Ltd. 

the element's edges:

$$u_h(x) = \sum_{K \in \mathscr{Q}_h} \sum_{E \subset \partial K} q_{K,E} w_{K,E}(x), \quad x \in \Omega$$

The two spaces $\mathscr{M}(\mathscr{Q}_h)$ and $\mathscr{N}(\mathscr{E}_h)$ are spanned, respectively, by the linearly independent scalar basis functions $\varphi_K$, $K \in (\mathscr{Q}_h)$, and $\lambda_E$, $E \in (\mathscr{E}_h)$, such that

$$\varphi_K(x) = \delta_{K,K'}, \quad x \in K', \ K, K' \in \mathscr{Q}_h$$

$$\lambda_E(x) = \delta_{E,E'}, \quad x \in E', \ E, E' \in \mathscr{E}_h$$

Thus, a function $p_h \in \mathscr{M}(\mathscr{Q}_h)$ (resp. $tp_h \in \mathscr{N}(\mathscr{E}_h)$) has one degree of freedom of constant value per element $K \in \mathscr{Q}_h$ (resp. $E \in \mathscr{E}_h$), such that

$$p_h(x) = \sum_{K' \in \mathscr{Q}_h} p_{K'} \varphi_{K'}(x) = p_K, \quad x \in K$$

$$tp_h(x) = \sum_{E' \in \mathscr{E}_h} tp_{E'} \lambda_{E'}(x) = tp_E, \quad x \in E$$

Now, we individually investigate the underlying equations in (6), which can be integrated over the element level.

*2.3.1. Discretization of Darcy's law.* By taking as test functions $\chi_K$ successively the basis functions $w_{K,E}$, the discretized equation of Darcy's law (the first equation in (6)) becomes

$$\int_K (\mathscr{K}_K^{-1} u_K) \cdot \chi_K \, \mathrm{d}x + \sum_{E \subset \partial K} \int_E tp_{K,E} \chi_K \cdot \nu_{K,E} \, \mathrm{d}\ell = \int_K p_K \nabla \cdot \chi_K \, \mathrm{d}x \tag{9}$$

where $\mathscr{K}_K$ is a piecewise approximation of the conductivity tensor over $K$, and

$$tp_E = tp_{K,E} = \begin{cases} tp_{K',E} & \text{if } E = K \cap K' \\ p_E^{\mathrm{D}} & \text{if } E \in \Gamma^{\mathrm{D}} \end{cases}, \quad E \in \mathscr{E}_h \cup \Gamma^{\mathrm{D}}, \ K, K' \in \mathscr{Q}_h$$

By integrating (9) and by making use of the Raviart–Thomas space basis properties, the following equations come into view:

$$\sum_{E' \subset \partial K} (B_K)_{E,E'} \ q_{K,E'} = p_K - tp_{K,E}, \quad E \subset \partial K, \ K \in \mathscr{Q}_h \tag{10}$$

In the matrix form, (9) is written as

$$B_K Q_K = p_K e - T_{P_K}, \quad K \in \mathscr{Q}_h \tag{11}$$

where $Q_K$ and $T_{P_K}$ are $N_K$-dimensional vectors containing, respectively, the fluxes $q_{K,E}$ and the traces of the pressure $tp_{K,E}$ on each $E \subset \partial K$, with $N_K$ being the number of edges of $K$; $e$ refers to the elementary divergence vector. It is of dimension $N_K$ and unitary entries and $B_K$ is an $N_K \times N_K$ symmetric positive-definite matrix whose elements are

$$(B_K)_{E,E'} = \int_K w_{K,E}^{\mathrm{T}} \ \mathscr{K}_K^{-1} \ w_{K,E'} \, \mathrm{d}x \tag{12}$$

It should be noted that these integrations are all evaluated exactly.

Copyright © 2002 John Wiley & Sons, Ltd. 

The last equation in (6) is equivalent to

$$\int_E u_K \cdot v_{K,E}\,\mathrm{d}\ell + \int_E u_{K'} \cdot v_{K',E}\,\mathrm{d}\ell = 0 \quad \text{if } E = K \cap K'$$

$$\int_E u_K \cdot v_{K,E}\,\mathrm{d}\ell = q_E^{\mathrm{N}} \quad \text{if } E \in \Gamma^{\mathrm{N}}$$

where $q_E^{\mathrm{N}} = \int_E q^{\mathrm{N}}\,\mathrm{d}\ell$.

Hence, the normal components of $u_h$ are continuous across the interelement boundaries, i.e.

$$q_{K,E} = \begin{cases} -q_{K',E} & \text{if } E = K \cap K' \\ q_E^{\mathrm{N}} & \text{if } E \in \Gamma^{\mathrm{N}} \end{cases} \tag{13}$$

By inverting the matrix $B_K$ and using (13), it is possible to eliminate the unknown flux. As a result, the reduced algebraic system, acquired by discretizing Darcy's law with unknowns the pressure head given in $P$ and its traces in $T_P$, becomes

$$R^{\mathrm{T}} P - M T_P + V = 0, \tag{14}$$

where $R^{\mathrm{T}}$ is the transpose matrix of $R$ which is a sparse matrix of dimension $N_{\mathscr{E}} \times N_{\mathscr{D}}$ with non-zero elements given by

$$(R)_{K,E} = \alpha_{K,E} = \sum_{E' \subset \partial K} (B_K^{-1})_{E,E'}, \quad E \subset \partial K$$

$M$ is an $N_{\mathscr{E}} \times N_{\mathscr{E}}$ sparse matrix with non-zero entries defined as

$$(M)_{E,E'} = \sum_{\partial K \supset E,E'} (B_K^{-1})_{E,E'}$$

$V$ is an $N_{\mathscr{E}}$-dimensional vector corresponding to the Dirichlet and Neumann boundary conditions.

*2.3.2. Discretization of the mass conservation equation.* By integrating the mass conservation equation (the second equation in (6)) where the test functions $\phi_h$ are successively replaced by the basis functions of $\mathscr{M}$, we get

$$s_K \mu_K \frac{\partial p_K}{\partial t} + \sum_{E \subset K} q_{K,E} = f_K, \quad K \in \mathscr{D}_h \tag{15}$$

where $s_K$ and $f_K$ are, respectively, the approximations of the storage coefficient and the sink/source term over $K$, $\mu_K$ denotes the measure of $K$.

Therefrom, by using (11) to replace the sum of fluxes in (15), we obtain an ordinary differential system which is given in its matrix form

$$S \frac{\mathrm{d}P}{\mathrm{d}t} + DP - RT_P = F \tag{16}$$

where $S$ is an $N_{\mathscr{D}} \times N_{\mathscr{D}}$ diagonal matrix with entries $(S)_{K,K} = \mu_K s_K$; $D$ is also an $N_{\mathscr{D}} \times N_{\mathscr{D}}$ diagonal matrix whose coefficients are

$$(D)_{K,K} = \alpha_K = \sum_{E \subset \partial K} \alpha_{K,E}$$

Copyright © 2002 John Wiley & Sons, Ltd. 

$F$ is a vector of dimension $N_2$, it corresponds to the source/sink function as well as to the imposed pressure given by the Dirichlet boundary conditions.

### *2.4. The derived algebraic system*

The spatial discretization of the governing equations obtained by applying the hybridized mixed formulation led to two systems. The first one, given in (14), is an algebraic system of unknowns $P$ and $T_P$ and the second is an ordinary system of first-order differential equations in time (16). By inverting the matrix $M$ which is symmetric, positive definite [6, 16, 18], it is possible to eliminate $T_P$ from (16) and consequently a stiff initial value problem is attained:

$$\begin{aligned} \frac{\mathrm{d}P}{\mathrm{d}t} &= LP + W \\ P(0) &= P^0 \end{aligned} \tag{17}$$

where

$$L = -S^{-1}(D - R^{\mathrm{T}}M^{-1}R), \quad W = R^{\mathrm{T}}M^{-1}V + F$$

The semi-exact solution (solution of the problem discretized in space with exact time integral operator) of (17) is given by the following formula:

$$P(t) = \mathrm{e}^{tL}P^0 + \int_0^t \mathrm{e}^{(t-s)L}W\,\mathrm{d}s \tag{18}$$

For simplicity, we assume that $p^{\mathrm{D}}$, $q^{\mathrm{N}}$ and $f$ are time-independent piecewise constant functions over the grid then $W$ is time independent and so (18) turns into

$$P(t) = \mathrm{e}^{tL}(P^0 + L^{-1}W) - L^{-1}W, \quad t \in [0, T] \tag{19}$$

This solution is computationally high priced due to the difficulties in evaluating the exponential besides inverting the matrix $M$. To avoid such problem, a temporal discretization of the differential operator in (16) is indispensable. Nevertheless, the solution given in (19) will be useful in appraising the accuracy of the time-discretization scheme. Since our primary motivation here is orientated to study the non-physical oscillations in the approximated pressure which is caused by the spatial discretization (as we will see later), a first-order accurate scheme for time discretization is adequate. Accordingly, the classical Euler backward (implicit) method is elected for the reason that it is unconditionally stable, besides it is easy to be carried out.

We subdivide $[0, T]$ into a finite number of equal subintervals of time steps $\Delta t$. By replacing the differential time operator in (16) by the difference quantity $(P^n - P^{n-1})/\Delta t$, then by simple substitution of $P^n$ in (14), the following system is achieved:

$$\begin{aligned} (M - \Delta t N)T_P^n &= RG^{-1}(SP^{n-1} + \Delta t F) + V \\ GP^n &= SP^{n-1} + \Delta t R^{\mathrm{T}}T_P^n + \Delta t F \end{aligned} \tag{20}$$

where $G = S + \Delta t D$, $N = RG^{-1}R^{\mathrm{T}}$.

Copyright © 2002 John Wiley & Sons, Ltd. 

Hence the problem is reduced to compute, at every time step, first $T_P$ by solving a linear system with symmetric, positive definite coefficient matrix $(M - \Delta t N)$ [18], then $P$ by solving a diagonal linear system. As a matter of fact, experimental inspections showed the adaptability and the robustness of the preconditioned conjugate gradient method in solving such systems [17].

## 3. PRESENTATION OF THE PROBLEM

Generally, the MHFE method is a wildly used tool to solve linear diffusion equations specially when both the pressure and the velocity of the flow are needed to be approximated. As a matter of fact, numerical laboratory works with this method furnished many phenomena where non-physical solutions are obtained and which are still inexplicable due to the complication of the initial–boundary values or the complexity of the underlying geometrical regions. For a better understanding of the problem, in this section we present a very simple well-posed initial–boundary value problem wherein various comparisons and observations of the numerical solution behaviour are interpreted.

The domain $\Omega$ is taken to be of rectangular shape $(0,20)\times(0,10)$ with the following initial–boundary conditions:

$$\begin{cases} s\dfrac{\partial p}{\partial t} + \nabla \cdot u = 0 & \text{in } \Omega \times (0,T] \\ u = -\mathscr{K}\nabla p & \text{in } \Omega \times (0,T] \\ p(x,0) = 0 & \text{in } \Omega \\ p = 1 & \text{on } \Gamma_1^{\mathrm{D}} \times (0,T] \\ p = 0 & \text{on } \Gamma_2^{\mathrm{D}} \times (0,T] \\ u.v = 0 & \text{on } \Gamma^{\mathrm{N}} \times (0,T] \end{cases} \tag{21}$$

where $\Gamma_1^{\mathrm{D}}$, $\Gamma_2^{\mathrm{D}}$ are, respectively, the left- and the right-hand perpendicular sides of the domain, $\Gamma_1^{\mathrm{D}} = \{0\}\times[0,10]$, $\Gamma_2^{\mathrm{D}} = \{20\}\times[0,10]$ and $\Gamma^{\mathrm{N}} = \partial\Omega\backslash\Gamma^{\mathrm{D}}$.

We discretize $\Omega$ into a $(20\times 10)$ uniform grid, the macro-elements are either rectangles or right angle triangles. In Figure 2, both together, the pressure $P$ and its traces $T_P$ are simulated over the grid with time step $\Delta t = T = 0.05$, $s = 1$ and $\mathscr{K} = 1$. It is clear that the two spatial discretization lead to severe peaks at some points of the solution. These oscillations cannot be evaded or disregarded since they even cause large critical deviations in the direction of the flow velocity, as appears in Figure 3. Even though this sample problem can be considered as a one-dimensional problem since physically the flow diffuses horizontally, the non-horizontal deviations of the flow velocity appearing in Figure 3(b) justify why the problem is discretized in the two-dimensional space. However, for the sake of clearness, in the runs the pressure will be visualized with one variable in space.

In Figure 4(a) we compare the approximated solutions of (21) obtained by applying the MHFE, FE and FD methods. We find that oscillatory solution is also obtained by the FE method except that these oscillations stay small compared to those obtained by the MHFEM.

Copyright © 2002 John Wiley & Sons, Ltd. 

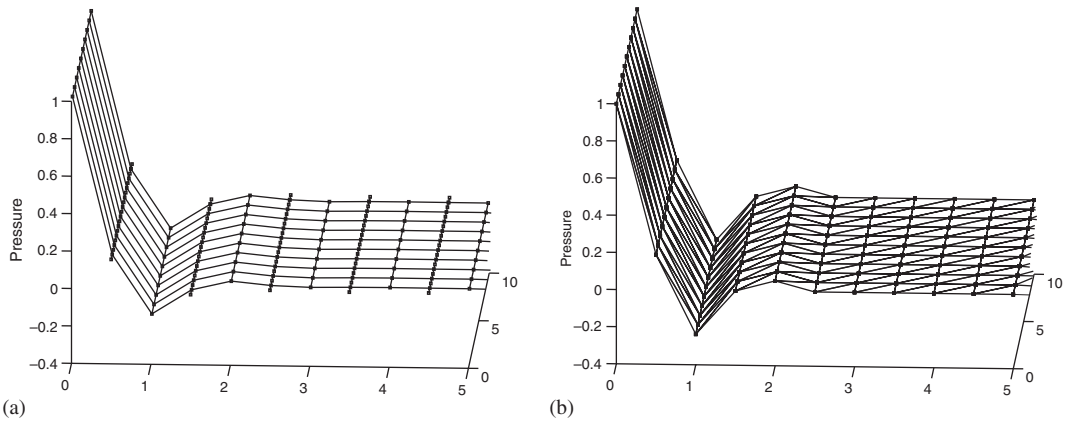


Figure 2. The pressure and its traces over the grid: (a) $20 \times 10$ grid of rectangular elements, $T = \Delta t = 0.05$; and (b) $20 \times 10$ grid of triangular elements, $T = \Delta t = 0.05$.

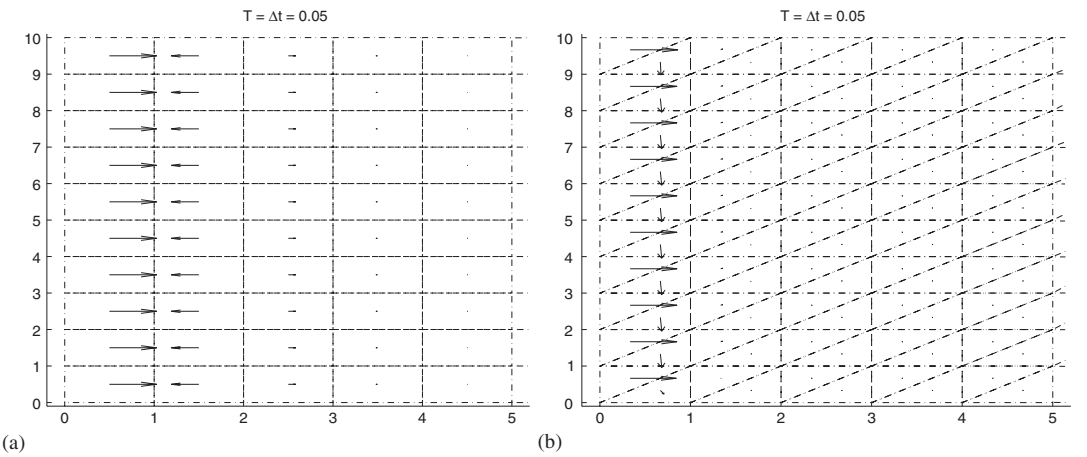


Figure 3. The velocity of the flow at the center of every element: (a) grid of $20 \times 10$ rectangular elements; and (b) grid of $20 \times 10$ triangular elements.

On the other hand, the finite difference method achieves a numerical solution free from any oscillations.

For an infinite long geometrical domain $\Omega$, the analytic solution of (21) is given by (see Reference [19])

$$p(x,t) = p^{\mathrm{D}} \operatorname{erfc}\left(\frac{x}{2\sqrt{t}}\right), \quad (x,t) \in [0,\infty) \times [0,\infty) \tag{22}$$

Copyright © 2002 John Wiley & Sons, Ltd. 

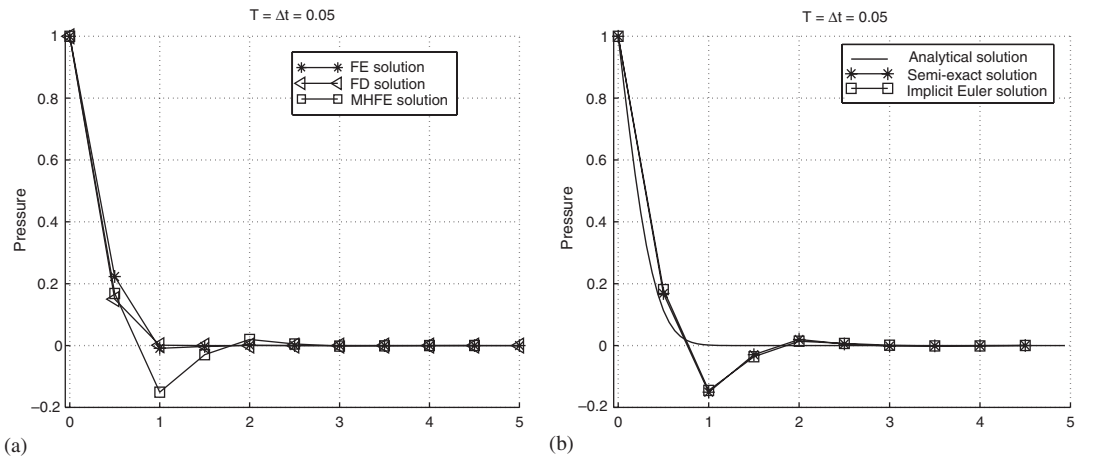


Figure 4. Comparisons between the analytical solution and the approximated solutions: (a) grid of $20 \times 10$ rectangular elements; and (b) grid of $20 \times 10$ rectangular elements.

where

$$\operatorname{erfc}(v) = 1 - \frac{2}{\sqrt{\pi}} \int_0^v \mathrm{e}^{-x^2}\, \mathrm{d}x, \quad v \in \mathbb{R}$$

By comparing the analytical solution (22), the semi-discretized time-dependent solution (19) and the Euler backward solution (20), as depicted in Figure 4(b), the following remarks are deduced.

- The sharp layer appearing in the analytic solution restricts its smoothness.
- Dis-convergences in the approximated solution occur in the region where large gradients in the analytical solution are located.
- The semi-exact solution is also oscillatory; moreover, it behaves in a similar manner as the Euler backward solution.

Since, in general, any discretizing scheme in time attempts to converge to the exact time-dependent solution, no time-discretizing method is able to amend these oscillations. Furthermore, if smaller time steps are taken the results may be even worse. Reasonably, we focus on the spatial decomposition of the domain. For the moment we try a uniform refinement of the mesh by taking a $(100 \times 10)$ grid. The depicted results in Figure 5(a) show that the MHFE method leads to an acceptable approximation of the exact solution. However, by trying out smaller time steps, oscillations will reappear again.

One more numerical test which will help to clarify this phenomenon is by increasing the simulation time interval $[0, T]$. In Figure 5(b), even though without any refinement of the mesh, convergence of the approximated pressure (similarly its derivative Figure 6) is attained and this is due to the intuitive nature of linear diffusion process whose solution becomes smoother as $t$ increases. It should be noted that similar oscillatory solutions may be also obtained if the sink/source function $f(x,t)$ varies abruptly in time.

As a primary conclusion, it becomes obvious to mind that in order to prevent any non-physical solutions it is advantageous to vary the mesh size in time and space according to

Copyright © 2002 John Wiley & Sons, Ltd. 

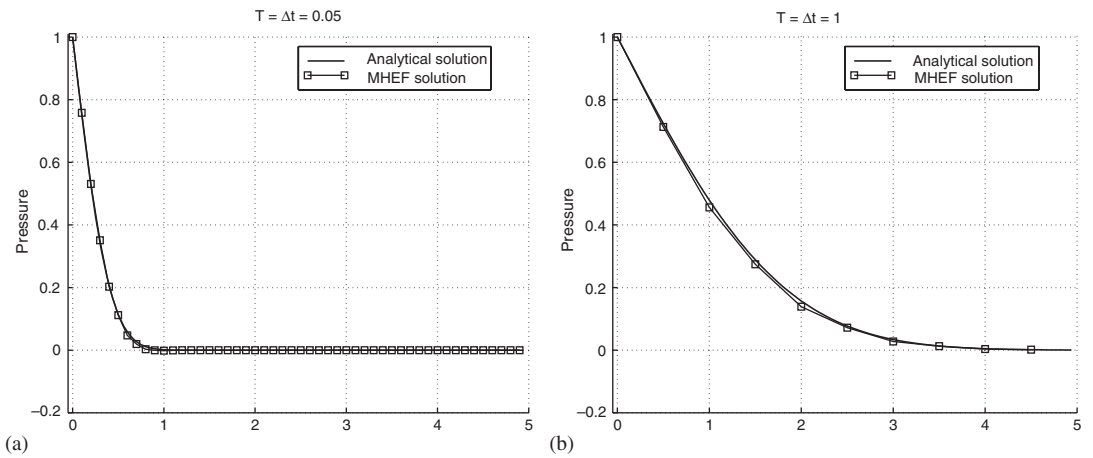


Figure 5. Reduction of space-step or enlargement of time interval wipes out oscillations: (a) $100 \times 10$ grid of rectangular elements; and (b) $20 \times 10$ grid of rectangular elements.

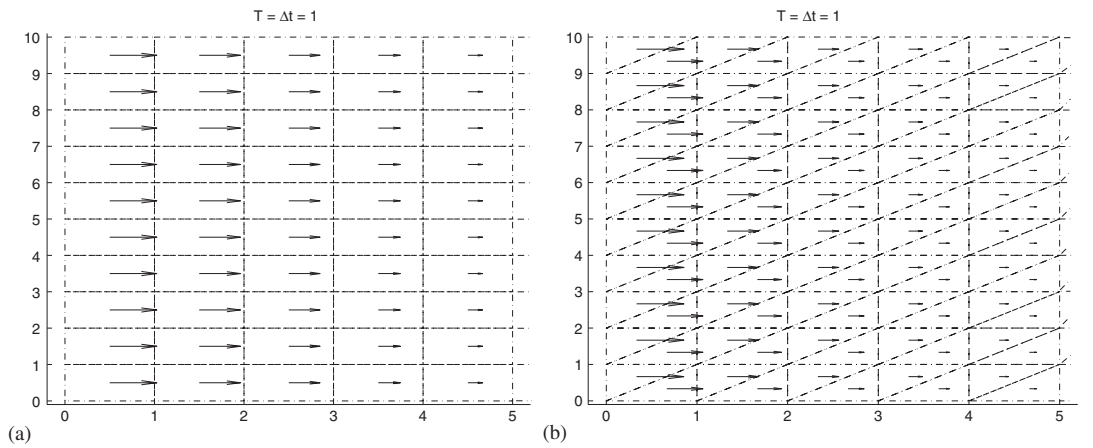


Figure 6. The velocity of the flow at the centre of every element: (a) $20 \times 10$ grid of rectangular elements; and (b) $20 \times 10$ grid of triangular elements.

the smoothness of the analytic solution. In the sequence, a criterion relating the temporal and spatial steps is presented whereby the domain can be discretized with maximum space steps and without oscillations in the solution.

## 4. DISCRETE MAXIMUM PRINCIPLE

The maximum principle is generally used to explore some information about the theoretical solution of some types of PDE. Specifically, it asserts that the solution cannot have a maximum

Copyright © 2002 John Wiley & Sons, Ltd. 

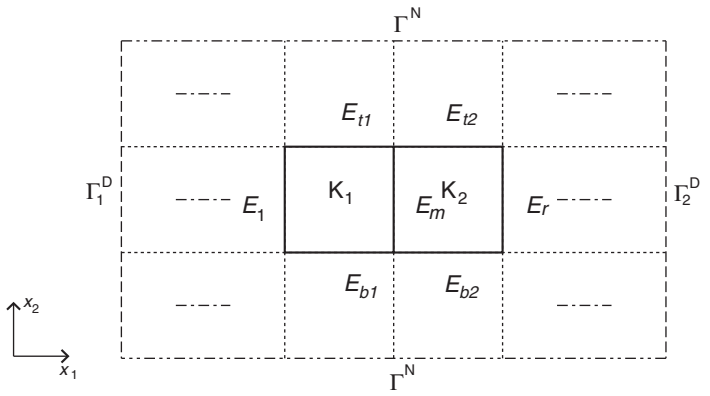


Figure 7. Two arbitrary adjacent element with their corresponding edges.

or a minimum within the interior of the underlying domain; besides, it is employed to show that the solution of certain problems must be non-negative. Accordingly, by applying the maximum principle to the problem given in (21), we obtain the following (see, e.g., References [20, 21]):

$$\begin{aligned} &\text{(i)} \quad \max_{\bar{\Omega}\times(0,T]} \{p(x,t)\} \leqslant \max_{\partial\Omega\times(0,T]} \{p(x,t),0\} \\ &\text{(ii)} \quad \min_{\bar{\Omega}\times(0,T]} \{p(x,t)\} \geqslant \min_{\partial\Omega\times(0,T]} \{p(x,t),0\} \end{aligned} \tag{23}$$

where $\bar{\Omega}=\Omega\cup\partial\Omega$.

So the pressure solution cannot have negative values as well as it is restricted between the Dirichlet boundary values. In the sequence, we verify whether the discrete maximum principle is obeyed by the discretized scheme given in (20) and this by investigating the following two properties:

$$(1)\ T_P^{n-1}\geqslant 0 \ \Rightarrow\ T_P^n\geqslant 0 \tag{24}$$

$$(2)\ \max(T_P^n)\leqslant \max(T_P^{n-1}) \tag{25}$$

We shall investigate the positivity of the scheme locally over each macro-element, i.e. $tp_{K,K}^{n-1}\geqslant 0 \Rightarrow tp_{K,E}^n\geqslant 0$ for $E\in\mathscr{E}_h, K\in\mathscr{Q}_h$. For the sake of simplicity, we shall introduce the case of uniform rectangular discretization of the mesh over homogenous isotropic medium such that $\mathscr{K}=aI,\ s=s_K\ \forall K\in\mathscr{Q}_h$, where $a$ is the anisotropic coefficient and $I$ is the $2\times 2$ identity matrix.

In Figure 7 we consider any two arbitrary adjacent elements in $\mathscr{Q}_h$. The local mass conservation property enables us to rewrite the hybridized mixed formulation over each element $K=K_1,\ K_2$. By inverting $B_K$ in (11) furnished from Darcy's law discretization, we get

$$q_{K,E}=a\left(\alpha_{K,E}\,p_K-\sum_{E'\subset\partial K}(B_K^{-1})_{E,E'}\,t\,p_{K,E'}\right)\forall E\subset\partial K,\ K=K_1,K_2 \tag{26}$$

Copyright © 2002 John Wiley & Sons, Ltd. 

$B_K$ can be simply obtained by exact integrations over each element $K$, its inverse is given by

$$B^{-1}=B_K^{-1}=2\begin{pmatrix} 2\dfrac{\Delta x_2}{\Delta x_1} & \dfrac{\Delta x_2}{\Delta x_1} & 0 & 0 \\ \dfrac{\Delta x_2}{\Delta x_1} & 2\dfrac{\Delta x_2}{\Delta x_1} & 0 & 0 \\ 0 & 0 & 2\dfrac{\Delta x_1}{\Delta x_2} & \dfrac{\Delta x_1}{\Delta x_2} \\ 0 & 0 & \dfrac{\Delta x_1}{\Delta x_2} & 2\dfrac{\Delta x_1}{\Delta x_2} \end{pmatrix} \tag{27}$$

From the spatial and the temporal discretization of the mass conservation equation, we obtain

$$p_K^n = p_K^{n-1} - \frac{\Delta t}{s\mu} \sum_{E\subset\partial K} q_{K,E}^n, \quad K=K_1,K_2 \tag{28}$$

Since there is no vertical diffusion of the flow, we have null fluxes across the horizontal edges, i.e.

$$q_{E_{\mathrm{t}1}}=q_{E_{\mathrm{b}1}}=q_{E_{\mathrm{t}2}}=q_{E_{\mathrm{b}2}}=0 \tag{29}$$

As depicted in Figure 7, the labels $\ell, \mathrm{r}, \mathrm{t}, \mathrm{b}$ and m refer to left, right, top, bottom and middle edges, respectively. Now by enforcing the continuity of the flux through the middle edge and by eliminating the unknowns $q_{K,E}$ (substitute (29) and (26) into (28)), the following system is achieved:

$$c_1 tp_{E_{\mathrm{m}}}^n = c_2(tp_{E_\ell}^n + tp_{E_r}^n) + c_3(p_{K_1}^{n-1} + p_{K_2}^{n-1}) \tag{30}$$

$$p_{K_1}^n = \frac{1}{1+2\lambda}\, p_{K_1}^{n-1} + \frac{\lambda}{1+2\lambda}\,(tp_{E_\ell}^n + tp_{E_{\mathrm{m}}}^n)$$

$$p_{K_2}^n = \frac{1}{1+2\lambda}\, p_{K_2}^{n-1} + \frac{\lambda}{1+2\lambda}\,(tp_{E_{\mathrm{m}}}^n + tp_{E_{\mathrm{r}}}^n) \tag{31}$$

where $\mu=\Delta x_1\Delta x_2, \alpha=\sum_{i=1,4} B_{i,1}^{-1}=6(\Delta x_2/\Delta x_1), \lambda=a\alpha\Delta t/s\mu, c_1=(B_{11}^{-1}+B_{22}^{-1}-2\alpha\lambda/(1+2\lambda))$, $c_2=(\alpha\lambda/(1+2\lambda)-B_{21}^{-1})$ and $c_3=\alpha/(1+2\lambda)$.

It is easy to verify that $c_1$ and $c_3$ are always non-negative, whereas $c_2$ is conditionally positive.

*Proposition 4.1*

The discrete maximum principle is satisfied by the MHFEM if $c_2$ is non-negative, i.e.

$$c_2 \geqslant 0 \;\Leftrightarrow\; \frac{\Delta x_1^2}{\Delta t} \leqslant \frac{6a}{s}$$

*Proof*

To verify the positivity of the scheme, the classical mathematical induction technique is utilized. We suppose that $tp_{K,E}^{n-1},\ p_K^{n-1}\geqslant 0$ and let us prove that $tp_{K,E}^n,\ p_K^n \geqslant 0\ \forall K\in\mathscr{D}_h, E\in\mathscr{E}_h$.

Copyright © 2002 John Wiley & Sons, Ltd. 

We denote by $\mathscr{E}^{\perp}$ the set of vertical edges of the mesh and $E_{\mathrm{m}} \in \mathscr{E}^{\perp}$ such that

$$tp^n_{E_{\mathrm{m}}} = \min\{tp^n_{K,E} \,|\, E \in \mathscr{E}^{\perp},\ K \in \mathscr{Q}_h\}$$

We shall only consider the non-trivial case, i.e. $E_{\mathrm{m}} \notin \Gamma^{\mathrm{D}}$. So $E_{\mathrm{m}}$ can be considered as an interior edge (suppose $E_{\mathrm{m}} = K_1 \cap K_2$). Consequently, by applying (30), we get

$$\begin{aligned} c_1 tp^n_{E_{\mathrm{m}}} &= c_2(tp^n_{E_\ell} + tp^n_{E_{\mathrm{r}}}) + c_3(p^{n-1}_{K_1} + p^{n-1}_{K_2}) \\ &\geqslant 2c_2 tp^n_{E_{\mathrm{m}}} + c_3(p^{n-1}_{K_1} + p^{n-1}_{K_2}) \quad (c_2, c_3 \geqslant 0) \end{aligned}$$

Since $(c_1 - 2c_2) \geqslant 0$ and $p^{n-1}_K$ are positive by our assumption then $tp^n_{E_{\mathrm{m}}} \geqslant 0$ and by making use of (31), one can deduce the positivity of $p^n_K$ for all $K \in \mathscr{Q}_h$. Now, if $E$ is a horizontal edge in $\mathscr{E}_h$ then one can easily deduce from (26) and (29) that $tp^n_{K,E}$ and $p^n_K$ have the same sign. Therefore, the positivity of the scheme holds. In order to avoid boring repetitions, similar technique can be used to verify the second property given in (25) by taking

$$tp^n_{E_{\mathrm{m}}} = \max\{tp^n_{K,E} \,|\, E \in \mathscr{E}^{\perp},\ K \in \mathscr{Q}_h\}$$ □

It should be noted that one can get the same results by verifying that the coefficient matrix $(M - \Delta t\, N)$ is an $M$-matrix. Since this matrix is symmetric definite positive then the $M$-matrix property holds by showing that the off-diagonal entries are non-positive [22]. As a result, in the general case of rectangular or uniform triangular grids, the MHFEM obeys the discrete maximum principle if the following criteria are satisfied for every $K \in \mathscr{Q}_h$:

$$\frac{(\Delta x_1^2)_K}{\Delta t} \leqslant \begin{cases} \dfrac{6a_K}{s_K} & \text{if } K \text{ is a rectangle} \\ \dfrac{6a_K}{\sqrt{2}s_K} & \text{if } K \text{ is a triangle} \end{cases} \tag{32}$$

The above criteria have a physical signification since the fraction $(a_K/s_K)(\mathrm{L}^2\mathrm{T}^{-1})$ is the so-called *diffusivity coefficient* [23]. Therefore, by logical inference, the space steps must not be larger than the *displacement pressure* in order to prevent negative solutions. It should be noted that similar criteria are also obtained in the case of standard Galerkin method; however, numerical experimentations showed that the non-physical oscillations obtained by this method are relatively less significant than those obtained by the MHFE method (see Figure 4). On the other hand, the classical finite difference method with one nodal degree of freedom seeks the approximated pressure by solving of the form a symmetric, definite positive penta-diagonal linear system. Hereby, one can easily verify that the discrete maximum principle is unconditionally obeyed by showing that the coefficient matrix is an $M$-matrix (see Reference [24]).

## 5. VARIOUS ALTERNATIVE APPROACHES TO PREVENT OSCILLATIONS

### 5.1. Refinement

The global refinement is maybe the simplest technique in order to enhance the accuracy of the approximated solution. As we have seen above, the criteria given in (32) enable us to refine the grid with maximum space steps (see Figure 8).

Copyright © 2002 John Wiley & Sons, Ltd. 

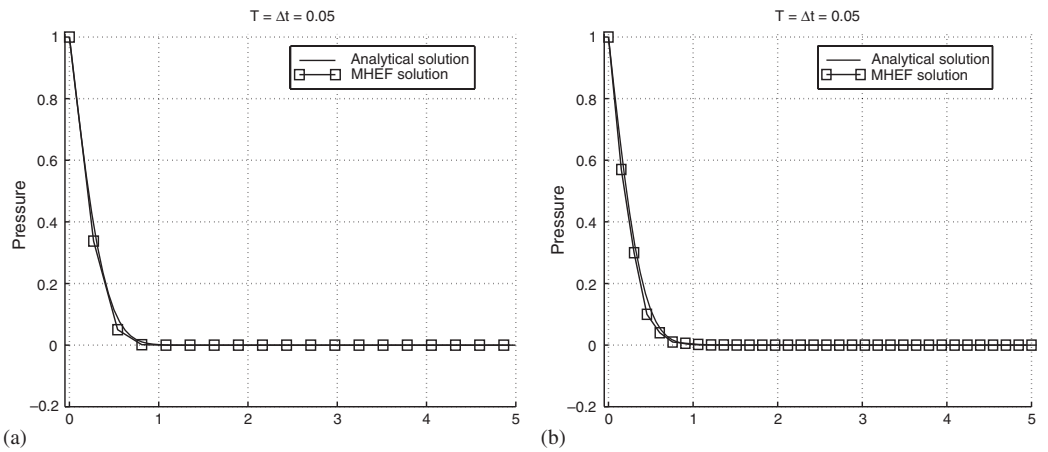


Figure 8. Global refinement of the grid by using the maximum allowed space step: (a) uniform grid of rectangular elements, $\Delta x_1 = (6\Delta t)^{1/2}$; and (b) uniform grid of triangular elements $\Delta x_1 = (3\times 2^{1/2}\Delta t)^{1/2}$.

Although speed and storage capabilities of computers have recently improved, the ever increasing demand to more time and memory requirements is endless. Owing to such circumspections, the global refinement technique may not be preferred in sizable problems.

### *5.2. Adaptive techniques*

In general, two types of adaptive techniques are mostly used; the first one is the local refinement method whereby uniform fine grids are added in the regions where the approximated solution lacks adequate accuracy, and the second is the moving mesh technique where nodes are relocated at necessary time steps.

We have found that the adaptive techniques could ameliorate the correctness of the solution despite the fact that their idea may not fit in with the conditions of the discrete maximum principle. However, we can define a process so that the discrete maximum principle is satisfied locally and precisely in the regions where high oscillations occur. Thereafter, we follow a similar work presented in Reference [25] where the mesh is moved so that a predetermined estimated error is satisfied and a system of differential equations is used to dominate the locations of the nodes. In our procedure, the error estimates rely on the properties given in (23) and the criteria previously discussed in (32) control the motion of the elements. Thus, we regroup the nodes (or add new nodes) in the regions where the solution behaves sharply in so that (32) are satisfied. However, in order to avoid non-smooth or coarse meshes, we uniformly redistribute the other nodes. By comparing Figures 4 and 9(a), one can clearly notice the improvement in the approximated solution achieved by the redistribution of the nodes. In Figure 9(b), we present the MHFE solution at different time simulations. It should be noted that the requisite solution with respect to the original grid can be simply obtained by linear interpolations.

### *5.3. Lumped-mass method*

By using the integration formula proposed in References [6, 26, 27] for rectangular elements and in Reference [28] for acute triangulations (the angles of triangular elements $\leqslant \pi/2$), the

Copyright © 2002 John Wiley & Sons, Ltd. 

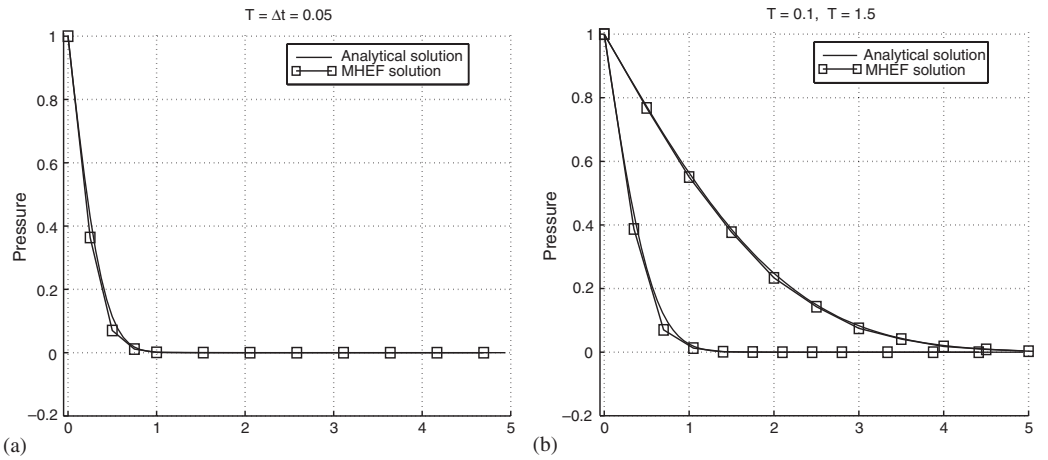


Figure 9. Relocating the mesh nodes at each time step; (a) non-uniform $20 \times 10$ grid of rectangular elements; (b) non-uniform $20 \times 10$ grids at different simulation times.

elementary matrix $B_K$ boils down to a diagonal matrix and so is $M$. Then the off-diagonal entries of $(M - \Delta tN)$ are

$$(M - \Delta tN)_{E,E'} = -\Delta t(RG^{-1}R^{\mathrm{T}})_{E,E'} \leqslant 0 \quad \forall E \neq E', E, E' \subset \mathscr{E}_h$$

Therefore, the coefficient matrix $(M - \Delta tN)$ is an $M$-matrix.

## 6. CONCLUSION

The mixed-hybrid finite-element methods have been developed to handle many physical models where the classical numerical methods such as the finite-element or the finite difference methods fail to give satisfactory representative approximations. The superior properties of this method is that it allows to conserve mass locally besides the primary unknown and its derivative are approximated simultaneously. In this work we have introduced a brief review of a non-conforming MHFE formulation corresponding to the lowest order Raviart–Thomas space which is the most popular. Due to the fact that the MHFEM does not obey the discrete maximum principle, many numerical experiments have brought to light some phenomena where non-physical oscillations are obtained. Accordingly, we have clearly seen such oscillations in the approximated solution of a simple artificial initial-boundary value problem by using rectangular and triangular grids. Consequently, a diffusivity criterion relating the space and time steps is given with respect to both spatial discretizations (rectangular and triangular grids). Some alternative solutions are suggested to solve this difficulty. The first natural remedy is a global or local refinement of the grid where we refine the mesh at necessary time steps in a way that we regroup the nodes in the regions where fast changes in the solution occur. The second idea is to use the mass-lumping technique whereby integrations are evaluated by using some approximation formula. Such techniques enable to reduce the MHFE method to

Copyright © 2002 John Wiley & Sons, Ltd. 

the finite difference or finite volume methods and in both cases the discrete maximum principle is obeyed.

## REFERENCES


1. Ackerer Ph, Younes A, Mose R. Modeling variable density flow and solute transport in porous medium: 1. Numerical model and verification. *Transport in Porous Media* 1999; **35**:345–373.
2. Yeh G. *Computational Subsurface Hydrology*: *Fluid Flows*. Kluwer Academic Publishers: The Pennsylvania State University, 1999.
3. Raviart PA, Thomas JM. *A Mixed Hybrid Finite Element Method for the Second Order Elliptic Problem*. Lectures Notes in Mathematics, vol. 606. Springer: New York, 1977; 292–315.
4. Brezzi F, Fortin M. *Mixed and Hybrid Finite Element Method*. Springer: New York, 1991.
5. Yotov I. Mixed finite element methods for flow in porous media. *Ph.D. Thesis*, University of Texas, 1996.
6. Chavent G, Roberts J-E. A unified physical presentation of mixed, mixed-hybrid finite element method and standard finite difference approximations for the determination of velocities in water flow problems. *Advances in Water Resources* 1991; **14**(6):329–348.
7. Arnold D, Brezzi F. Mixed and nonconforming finite element methods: implementation, postprocessing and error estimates. *RAIRO Modélisation Mathematique Analyse Numérique* 1985; **19**:7–32.
8. Arbogast T, Wheeler M, Yotov I. Mixed finite elements for elliptic problems with tensor coefficients as cell-centered finite differences. *SIAM Journal on Numerical Analysis* 1997; **34**(2):828–852.
9. Nakata M, Weiser A, Wheeler M. Some superconvergence results for mixed finite elements for elliptic problems on rectangular domains. *The Mathematics of Finite Elements and Applications*. Academic Press: London, 1985; 367–389.
10. Hennart J-P. Nodal schemes, mixed-hybrid finite elements and block-centered finite differences. *Rapport de Recherche INRIA*, No. 386, 1985.
11. Mose R, Siegel P, Ackerer Ph, Chavent G. Application of the mixed-hybrid finite element approximation in a ground water flow model: luxury or necessity? *Water Resources Research* 1994; **30**(11):3001.
12. Durlofsky L. Accuracy of mixed and control volume finite element approximations to Darcy velocity and related quantities. *Water Resources Research* 1994; **30**(4):965.
13. Thomas J. Sur l'Analyse Numérique des Méthodes d'Elément Finis Hybrides et Mixtes. *Thèse de Doctorat d'Etat*, Univ. de Pierre et Marie Curie, 1977.
14. Johnson C, Thomée V. Error estimates for some mixed finite element methods for parabolic type problems. *RAIRO Analyse Numérique* 1981; **15**:41–78.
15. Brezzi F, Marini L, Pietra P. Two-dimensional exponential fitting and applications to drift–diffusion models. *SIAM Journal on Numerical Analysis* 1989; **26**(6):1342–1355.
16. Chavent G, Jaffré J. *Mathematical Models and Finite Elements for Reservoir Simulation*. Elsevier Science: Netherlands, 1986.
17. Kaasschieter E, Huijben A. Mixed-hybrid finite elements and streamline computation for the potential flow problem. *TNO-Report PN* 90-02-A, TNO Institute of Applied Geoscience, 1990.
18. Hoteit H, Erhel J, Mosé R. Numerical reliability and time requirements for the mixed methods applied to flow problems in porous media. *Computational Geosciences*, to appear.
19. Carslaw H, Jaeger J. *Conduction of Heat in Solids.* Clarendon: Oxford, 1959;363–365.
20. Protter M, Weinberger H. *Maximum Principles in Differential Equations*. Prentice-Hall Partial Differential Equations Series. Prentice-Hall: Englewood cliffs, NJ.
21. Renardy M, Rogers R. *An Introduction to Partial Differential Equations*. Springer: New York.
22. Windisch G. *M*-matrices in numerical analysis. *Teubner-Texte zur Mathematikische*:115,1989.
23. Marsily G. *Hydrogéologie Quantitative*. Masson: Paris, 1981.
24. Amiez G, Gremand P. On a numerical approach of Stefan-like problems. *Numerische Mathematik* 1991; **59**: 71–89.
25. Adjerid S, Flaherty J. A moving finite element method with error estimation and refinement for one-dimensional time dependent partial differential equations. *SIAM Journal on Numerical Analysis* 1986; **23**(4):778–796.
26. Russell T, Wheeler M. Finite element and finite difference methods for continuous flows in porous media. In *The Mathematics of Reservoir Simulation*, Ewing R (ed.), SIAM: Philadelphia, PA, 1983; 35–106.
27. Arbogast T, Wheeler M, Yotov I. Enhanced cell-centered finite differences for elliptic equations on general geometry. *SIAM Journal on Scientific Computing* 1998; **19**:404–425.
28. Baranger J, Maitre JF, Oudin F. Convection between finite volume and mixed finite element methods. *Equipe d'analyse Numerique Lyon Saint-Etienne* No. 198, 1995.


Copyright © 2002 John Wiley & Sons, Ltd. 